

24 **ABSTRACT**

25 Archaeal swimming motility is driven by rotary motors called archaella. The structure of these
26 motors, and particularly how they are anchored in the absence of a peptidoglycan cell wall, is
27 unknown. Here, we use electron cryotomography to visualize the archaellar motor *in vivo* in
28 *Thermococcus kodakaraensis*. Compared to the homologous bacterial type IV pilus (T4P), we
29 observe structural similarities as well as several unique features. While the position of the
30 cytoplasmic ATPase appears conserved, it is not braced by linkages that extend upward through
31 the cell envelope as in the T4P, but rather by cytoplasmic components that attach it to a large
32 conical frustum up to 500 nm in diameter at its base. In addition to anchoring the lophotrichous
33 bundle of archaella, the conical frustum associates with chemosensory arrays and ribosome-
34 excluding material and may function as a polar organizing center for the coccoid cells.

35

36 INTRODUCTION

37 Motility is a fundamental property of single-celled organisms. In archaea, swimming motility is
38 driven by a rotary motor called the archaellum. Archaella are functionally analogous to bacterial
39 flagella, but evolutionarily homologous to the type IV pilus (T4P) and type II secretion system
40 (T2SS) machineries of bacteria [1]. Recently, an atomic structure of the archaellum fiber
41 purified from the euryarchaeon *Methanospirillum hungatei* revealed differences compared to the
42 bacterial T4P fiber, including lack of a central pore and more extensive inter-subunit interactions
43 [2]. The structure of the archaellar basal body, and its similarity to the T4P basal body remains
44 unknown.

45
46 Unlike T4P fibers that only assemble and disassemble, archaella assemble and can then rotate in
47 both directions to either push or pull the cell [3, 4]. Light microscopy of *Halobacterium*
48 *salinarum* revealed discrete steps during rotation, likely corresponding to ATP hydrolysis events
49 by the basal body ATPase, FlaI [5]. While the bacterial T4P contains two distinct ATPases for
50 assembly and disassembly of the pilus fiber, the single ATPase FlaI drives both assembly and
51 rotation of the archaellum [6]. The N-terminal domain of the archaellum/T2SS/T4P superfamily
52 ATPases is the most variable, and the first 29 residues of FlaI, located on the outer edge of the
53 hexamer, were found to be essential for motility but not assembly, although the basis of this
54 functional separation remains unclear [6].

55
56 FlaI is predicted to interact with the integral membrane protein FlaJ [7]. Structural studies of the
57 bacterial T4P suggest that ATPase-driven rotation of the FlaJ homolog, PilC, incorporates pilin
58 subunits from the membrane into the growing fiber [8]. This is possible because the ATPase

59 itself is clamped in an integrated structure that spans the inner and outer membranes and
60 periplasm and anchors on the cell-encompassing peptidoglycan cell wall [8]. A similar cell-wall-
61 attached structure anchors the rotation of the bacterial flagellar motor [9]. Without knowing the
62 structure of the archaeellar basal body, it is unclear how similar anchoring could occur in the
63 envelope of archaea, which consists of a single membrane and thin proteinaceous surface (S-
64)layer. It was recently proposed that FlaF might anchor the archaeellum through interactions with
65 the S-layer [10]. Others have suggested that a cytoplasmic structure mechanically stabilizes the
66 motor [3]. Supporting this idea, cytoplasmic structures underlying the archaeella have been
67 observed by traditional electron microscopy (EM) of Halobacteria [11, 12].

68
69 Electron cryotomography (ECT) can image intact cells in a frozen, fully-hydrated state,
70 providing macromolecular-resolution (~4-6 nm) details about native cellular structures [13].
71 Here, we used ECT to visualize the structure of the archaeellar basal body *in vivo* in
72 *Thermococcus kodakaraensis* cells. *T. kodakaraensis* (originally designated *Pyrococcus* sp.
73 strain KOD1 and later identified as belonging to the *Thermococcus* genus [14]; also known as *T.*
74 *kodakarensis*) is one of the best-studied archaeal species. It was isolated from a Japanese
75 solfatara in 1994 [15], and has proven readily amenable to genetics (well-developed gene
76 manipulation techniques exploit its natural competence [16]) and the isolation of thermostable
77 enzymes (e.g. high-fidelity DNA polymerase for PCR [17]). In addition to revealing the overall
78 structure of the archaeellar basal body *in vivo*, we discovered a novel cytoplasmic conical
79 structure in *T. kodakaraensis* associated with archaeellar motility and potentially other polar
80 organizing activities.

81

82 RESULTS

83 We imaged *T. kodakaraensis* cells by ECT in a native, frozen-hydrated state. Many cells
84 appeared to be lysed prior to plunge-freezing for ECT, but out of 18 apparently intact cells, we
85 observed a lophotrichous bundle of archaella in 13. Each bundle contained between four and 14
86 archaella. Due to the relatively large size of *T. kodakaraensis* cells (cells are irregular cocci ~1.5
87 μm in diameter), only a portion of the cell was visible in the limited field of view of our high-
88 magnification cryotomograms. We therefore think it likely that in the remaining five cells, the
89 archaellar bundle was present but not located in the portion of the cell imaged. In addition, we
90 observed well-preserved archaellar bundles in eight apparently lysed cells.

91
92 We consistently observed a prominent conical structure associated with the archaellar bundle in
93 the cytoplasm (Figure 1). We never observed archaella unassociated with a cone, or vice versa.
94 The conical structure showed a consistent morphology and localization inside the cell: closely
95 associated with, but not touching, the cytoplasmic membrane at its narrow end and expanding a
96 variable length to a wide base, which varied from 220 to 525 nm in diameter. The central axis
97 was perpendicular to the membrane, as seen in cross-sectional side views (Figure 1A-C,
98 additional examples in Figure EV1). The edges, seen in cross-section, frequently exhibited
99 periodic densities suggestive of individual protein subunits (Figure 1C), with a thickness of 3-4
100 nm. We observed that while cones in different cells had different heights, the opposite edges
101 within each cone were always symmetric (of similar lengths). Tomographic slices capturing the
102 central axis of the conical structure in side view showed an angle of $109 \pm 6^\circ$ (mean \pm s.d., n=5)
103 between opposite edges. The structures were not complete cones but rather conical frusta: they
104 did not taper fully to a point, but exhibited a blunt tip. In top-views, we observed a ring situated

105 in the throat of the frustum, just below the tip (Figure 1D,E). These rings comprised 19 subunits
106 (Figure 1D inset), each again 3-4 nm thick, with an overall ring diameter of 31 ± 2 nm (mean \pm
107 s.d., n=10). The position of the ring in the conical frustum was clearest in tomograms of lysed
108 cells, which were thinner and contained less cytoplasmic material (Figure 1F-H). Even in such
109 tomograms, however, we could not visualize a well-defined connection between the two portions
110 of the structure, so it is unclear if and how the components are connected.

111
112 Conical structures were surrounded by an \sim 30-45 nm wide ribosome-excluding zone (REZ)
113 (Figure 1E, Figure 2). In nearly all cells, both intact and lysed, we observed filament bundles
114 near or associated with this REZ (Figure 2B-E). The bundles were more extensive in lysed cells.
115 Each filament was \sim 12 nm wide and made up of a series of disk-like densities spaced \sim 7 nm
116 apart. Chemosensory arrays were also consistently observed near the conical structures (Figure
117 2A,B). In one cell, we observed two attached conical structures, each associated with archaella
118 and each approximately 250 nm in diameter at its base (Figure EV2).

119
120 To characterize the interaction between the archaellar bundle and the conical structure, we
121 measured the distance from the base of each archaellum in the membrane to the cone. The
122 structure of the cone means that the distance between it and the membrane varies – shortest at the
123 tip of the cone and longest at the base. Since archaella were located at various radial positions
124 along the cone, we expected their distance to vary similarly. Interestingly, however, we
125 measured a much more consistent distance of 44 ± 5 nm (mean \pm s.d., n=29) from the cone to the
126 base of each archaellum in the membrane (Figure 3). Consistent with this, we observed a variety
127 of orientations of archaella in the cell envelope, frequently not perpendicular to the S-layer,

128 allowing the conserved distance to the cone (Figure 3, Figure EV3). In a few cases, we observed
129 continuous densities connecting the archaella and the cone (Figure EV3E).

130
131 To determine the structure of the archaellar basal body, we calculated a subtomogram average
132 (Figure 4). 30 particles were used, and an axial two-fold symmetry was applied. The resulting
133 average revealed several layers of density extending into the cytoplasm. Immediately adjacent to
134 the membrane-embedded density was a ring-like structure (L1 in Figure 4A). Below the ring
135 was a disk of similar diameter (L2), followed by a larger diameter component (L3) and finally, at
136 a greater distance, a less well-defined density. This density was 44 nm away from the
137 membrane, corresponding to the cone. Consistent with our observation that archaella exhibited
138 various orientations with respect to the S-layer, we did not observe a strong density
139 corresponding to the S-layer in the average. As seen in individual particles, the component in L3
140 does not appear to be a ring, but rather comprises distinct legs, seen on one or both sides, that
141 appear symmetric in the average (Figure EV4). Similarly, the density of the cone is more
142 prominent in individual particles; different angles of the structure in different particles wash out
143 in the average (Figure EV4).

144

145 **DISCUSSION**

146 ***Structure of the basal body of the T. kodakaraensis archaellum***

147 Here we describe the structure of the archaellar motor in *T. kodakaraensis* (Figure 4). We think
148 it is almost certain that density L1 in the *T. kodakaraensis* basal body corresponds to the ATPase,
149 FlaI, since its size and shape match those of the homologous ATPases in the T4P and all three
150 interact directly with integral membrane proteins. More specifically, FlaI shares domain

151 homology with the assembly/disassembly ATPases, PilB and PilT, of the bacterial T4P. The size
152 of L1 is comparable to that of the PilB/PilT ring in the bacterial T4P (Figure 4B), consistent with
153 their conserved hexameric oligomerization [7] and similar sizes of the protein monomers (540
154 amino acids for FlaI and 566 for PilB). FlaI is predicted to interact directly with the polytopic
155 integral membrane protein FlaJ [6, 7]. FlaJ shares sequence homology with the ATPase-
156 interacting inner membrane protein PilC of the T4P [18]. The relative locations of these
157 components are therefore predicted to be the same in the basal bodies of the archaeellum and the
158 bacterial T4P (Figure 4) [8, 19], and the size and shape and position of density L1 seen here
159 support that expectation, and the corollary that these two systems likely share a similar assembly
160 mechanism.

161
162 The identities of the proteins making up L2, L3, and the cone remain unclear. In the T4P, no
163 structures were observed in the cytoplasm below the ATPase [8, 19, 20]. In Crenarchaeota, only
164 one accessory component is not membrane-bound (FlaH). In Euryarchaeota like *T.*
165 *kodakaraensis*, however, additional soluble proteins, FlaC/D/E, are thought to be components of
166 the archaeellum that receive switching signals from the chemotaxis machinery [21]. All of these
167 proteins, and potentially others, are candidates for the densities we observed. It will therefore be
168 of great interest to obtain a structure of the crenarchaeal basal body, which lacks FlaC/D/E, for
169 comparison, and/or to dissect the *T. kodakaraensis* basal body structure through analysis of
170 deletion mutants.

171

172 ***Conical structures anchor T. kodakaraensis archaeella***

173 We observed that *T. kodakaraensis* archaella associate with a large conical structure in the
174 cytoplasm. In a few cases, we observed direct connections between archaella and cone. The fact
175 that we did not see such a connection for every archaellum may simply reflect variations in
176 image clarity and orientation of the structures between cells in different cryotomograms. The
177 conserved distance from the cone to the archaellar basal body in the membrane suggests a rigid
178 interaction. It is an interesting question how archaella are attached to the cone. We did not
179 observe strong densities connecting L3 and the cone in the averaged basal body structure, but in
180 individual particles we observed heterogeneity. Also, the resolution of the average may be too
181 low to detect such connections. If, for example, the links are thin (such as coiled-coils), they
182 would not be resolved; similar coiled-coil linkages in the bacterial flagellar motor between FlaH
183 and the C-ring were not resolved even in higher-resolution subtomogram averages [22].

184
185 We propose that the *T. kodakaraensis* cone anchors the archaellar basal body in part to provide
186 leverage for rotation. In the bacterial T4P, the ATPase is clamped by extensive interactions up
187 through the cell envelope that anchor it to the peptidoglycan cell wall [8] (Figure 5). Signals
188 governing disassembly are thought to be processed by sensory elements in the periplasm [8]. In
189 the absence of a peptidoglycan cell wall and outer membrane, the *T. kodakaraensis* archaellum
190 appears to turn the system upside down, with components stacking nearly 50 nm into the
191 cytoplasm to anchor onto a large cone (Figure 5). Signals governing rotation and direction are
192 likely integrated by sensory components in the cytoplasm.

193
194 Similar leveraging structures may exist in other Archaea. More than twenty years ago, it was
195 observed that when archaella are dissociated from lophotrichous *H. salinarum* cells by detergent,

196 the bundles remain intact, connected to a large (~500 nm diameter) structure [11]. A similar
197 structure was also observed below the cell membrane in cell ghosts [12]. More recently, a
198 spherical structure was observed anchoring Iho670 fibers, T4P-like filaments in *Ignicoccus*
199 *hospitalis*. This structure is thought to be located in the cytoplasm of the cell and contains a
200 central ring of similar dimensions to the one observed here [23]. It is possible that either or both
201 of these structures are related to the *T. kodakaraensis* cone. Large cytoplasmic structures have
202 not been described in other motile archaeal species to date, however, so it will be interesting to
203 determine how archaella may be anchored in those systems.

204
205 It will also be of great interest to identify the proteins that form the *T. kodakaraensis* cone and
206 associated ring. These subunits must be capable of interacting both circumferentially around the
207 cone as well as radially with subunits making up the next (larger or smaller diameter) ring.
208 While it is possible that the conical structure is an assembly of stacked rings, we think it more
209 likely that the subunits assemble into a filament spiral, similar to what has been proposed for
210 ESCRT-III polymers [24, 25]. Interestingly, an architecturally similar spiral has been observed
211 in the basal body of the bacterial flagellar motor: in *Wolinella succinogenes*, an Archimedian
212 spiral forms a bushing for the motor in the periplasm, allowing the flagellum to rotate in the cell
213 wall. This spiral is formed by protein subunits interacting both circumferentially and laterally
214 through nonspecific interactions [26]. While that spiral takes the form of a disk, similar protein
215 interactions may give rise to a cone in *T. kodakaraensis*.

216

217 ***T. kodakaraensis* cones are potential polar organizing structures**

218 In addition to a potential role in rigidly anchoring the basal body of the archaellum, the *T.*
219 *kodakaraensis* cone may function to gather the archaellar bundle to maximize efficiency, either
220 by concentrating molecules for assembly or signaling, or by concentrating force at one point on
221 the coccoid cell for directional swimming. The cone's structure may also help distribute the
222 force from archaellar rotation to the larger bulk of the cell's contents. This might be more
223 efficient in a pushing than a pulling mode; swimming speed in another euryarchaeon, *H.*
224 *salinarum*, was found to be approximately twice as fast when the archaella push as when they
225 pull the cell body [5]. The structurally-similar spiral basal disk in the bacterial flagellar motor of
226 *W. succinogenes* was suggested to play a role in dispersing lateral forces created by flagellar
227 rotation [26].

228
229 Our results suggest a further role for the cone in breaking the symmetry of the coccoid cell. In
230 many rod-shaped bacterial cells, proteins and other macromolecules are specifically localized to
231 the cell pole for various purposes ranging from cell motility and adhesion to differentiation and
232 division [27]. One well-studied example of this polar organization occurs in *Caulobacter*
233 *crescentus*, where the oligomeric protein PopZ defines an asymmetric pole, localizing many
234 cytoplasmic proteins and tethering the chromosomal centromere to facilitate division [28-30]. In
235 *Vibrio cholerae*, the HubP protein organizes the polar localization of the chromosomal origin,
236 chemotaxis machinery, and flagella [31]. Perhaps the *T. kodakaraensis* cone similarly defines a
237 pole in the spherical cells, anchoring the chemotaxis and motility machinery. An intriguing
238 feature observed in our cryotomograms is the cone-associated REZ. In bacterial cells, such
239 REZs are commonly interpreted to be the nucleoid [32, 33]. Supporting this assignment, we
240 observed bundles of filaments (most extensive in lysed cells) associated with the REZ (Figure 2).

241 Such filaments are reminiscent of nucleoprotein filaments formed by various bacterial DNA-
242 binding proteins in stress conditions [34-36].

243
244 A spatial organizer analogous to PopZ may be especially important for a polyploid species like
245 *T. kodakaraensis* (chromosome copy number varies depending on growth phase, from 7 to 19
246 copies [37]). Fluorescence imaging suggests that the nucleoid is relatively compact in log phase
247 growth, and nucleoids appear to separate before the cells are deeply constricted [38]. Perhaps
248 the cones segregate attached structures, including the archaella and possibly chromosomes. This
249 function is consistent with the duplicated cone structure we observed in one cell (Figure EV2),
250 which could represent an intermediate after replication and prior to segregation, or may simply
251 represent an aberrant structure. Further studies imaging cells throughout the cell cycle could
252 shed light on whether, and how, cones function to coordinate archaellar and chromosomal
253 segregation.

254
255 Understanding the prevalence of this structure among Euryarchaeota and across different
256 archaeal kingdoms may illuminate its function. If it is restricted to lophotrichous species, it may
257 simply be an anchoring mechanism for the archaella in the absence of a peptidoglycan cell wall.
258 In that case, monotrichous or peritrichous species may exhibit a less extensive plate underneath
259 the basal bodies of individual archaella. If it is more widely found in coccoid, and/or highly
260 polyploid, cells, it may serve an added role in polar specification.

261

262 **METHODS**

263 ***Growth***

264 *Thermococcus kodakaraensis* strain KOD1 [JCM 12380] was grown anaerobically in MA-YT
265 medium supplemented with elemental sulfur as previously described [14, 39].

266

267 ***Electron cryotomography and image analysis***

268 Samples of cell cultures in growth media were mixed with bovine serum albumin-treated
269 colloidal gold fiducial markers (Sigma) and applied to Quantifoil R2/2 200 copper EM grids
270 (Quantifoil Micro Tools). After blotting excess liquid, grids were plunge-frozen in a mixture of
271 liquid ethane and propane [40], and subsequently kept at liquid nitrogen temperature. Images
272 were acquired using either an FEI Polara G2 or Titan Krios 300 keV transmission electron
273 microscope (FEI Company) equipped with a field emission gun, image corrector for lens
274 aberration, energy filter (Gatan), and K2 Summit direct electron detector (Gatan). Cumulative
275 electron dose was $160 \text{ e}^-/\text{\AA}^2$ or less for each tilt-series. Tilt-series were acquired using UCSF
276 Tomography software [41]. Images were contrast transfer function corrected, aligned, and
277 reconstructed by weighted back projection with the IMOD software package [42]. SIRT
278 reconstructions were calculated with TOMO3D [43], subtomogram averages generated using
279 PEET [44], and segmentations generated with Amira software (FEI Company).

280

281 **ACCESSION CODES**

282 The subtomogram average of the *T. kodakaraensis* archaeellar basal body was deposited into the
283 Electron Microscopy Data Bank (entry number EMD-8603).

284

285 **ACKNOWLEDGMENTS**

286 This work was supported by the NIH (grants R01GM101425 and R01AI127401 to G.J.J.) and
287 the UCLA-DOE Institute (grant DE-FC03-02ER26342 to R.P.G.).

288

289 REFERENCES

- 290 1. Pohlschroder, M., et al., *Archaeal type IV pilus-like structures--evolutionarily conserved*
291 *prokaryotic surface organelles*. Curr Opin Microbiol, 2011. **14**(3): p. 357-63.
- 292 2. Poweleit, N., et al., *CryoEM structure of the Methanospirillum hungatei archaeellum*
293 *reveals structural features distinct from the bacterial flagellum and type IV pilus*. Nat
294 Microbiol, 2016. **2**: p. 16222.
- 295 3. Alam, M. and D. Oesterhelt, *Morphology, function and isolation of halobacterial*
296 *flagella*. J Mol Biol, 1984. **176**(4): p. 459-75.
- 297 4. Shahapure, R., et al., *The archaeellum: a rotating type IV pilus*. Mol Microbiol, 2014.
298 **91**(4): p. 716-23.
- 299 5. Kinoshita, Y., et al., *Direct observation of rotation and steps of the archaeellum in the*
300 *swimming halophilic archaeon Halobacterium salinarum*. Nat Microbiol, 2016. **1**(11): p.
301 16148.
- 302 6. Reindl, S., et al., *Insights into FlaI functions in archaeal motor assembly and motility*
303 *from structures, conformations, and genetics*. Mol Cell, 2013. **49**(6): p. 1069-82.
- 304 7. Ghosh, A. and S.V. Albers, *Assembly and function of the archaeal flagellum*. Biochem
305 Soc Trans, 2011. **39**(1): p. 64-9.
- 306 8. Chang, Y.W., et al., *Architecture of the type IVa pilus machine*. Science, 2016.
307 **351**(6278): p. aad2001.
- 308 9. Murphy, G.E., J.R. Leadbetter, and G.J. Jensen, *In situ structure of the complete*
309 *Treponema primitia flagellar motor*. Nature, 2006. **442**(7106): p. 1062-4.
- 310 10. Banerjee, A., et al., *FlaF Is a beta-Sandwich Protein that Anchors the Archaeellum in the*
311 *Archaeal Cell Envelope by Binding the S-Layer Protein*. Structure, 2015. **23**(5): p. 863-
312 72.
- 313 11. Kupper, J., et al., *The flagellar bundle of Halobacterium salinarium is inserted into a*
314 *distinct polar cap structure*. J Bacteriol, 1994. **176**(16): p. 5184-7.
- 315 12. Metlina, A.L., *Bacterial and archaeal flagella as prokaryotic motility organelles*.
316 Biochemistry (Mosc), 2004. **69**(11): p. 1203-12.
- 317 13. Oikonomou, C.M. and G.J. Jensen, *A new view into prokaryotic cell biology from*
318 *electron cryotomography*. Nat Rev Microbiol, 2016. **14**(4): p. 205-20.
- 319 14. Atomi, H., et al., *Description of Thermococcus kodakaraensis sp. nov., a well studied*
320 *hyperthermophilic archaeon previously reported as Pyrococcus sp. KOD1*. Archaea,
321 2004. **1**(4): p. 263-7.
- 322 15. Morikawa, M., et al., *Purification and characterization of a thermostable thiol protease*
323 *from a newly isolated hyperthermophilic Pyrococcus sp.* Appl Environ Microbiol, 1994.
324 **60**(12): p. 4559-66.
- 325 16. Hileman, T.H. and T.J. Santangelo, *Genetics Techniques for Thermococcus kodakarensis*.
326 Front Microbiol, 2012. **3**: p. 195.

- 327 17. Hashimoto, H., et al., *Crystal structure of DNA polymerase from hyperthermophilic*
328 *archaeon Pyrococcus kodakaraensis KOD1*. J Mol Biol, 2001. **306**(3): p. 469-77.
- 329 18. Peabody, C.R., et al., *Type II protein secretion and its relationship to bacterial type IV*
330 *pili and archaeal flagella*. Microbiology, 2003. **149**(Pt 11): p. 3051-72.
- 331 19. Chang, Y.W., et al., *Architecture of the Vibrio cholerae toxin-coregulated pilus machine*
332 *revealed by electron cryotomography*. Nat Microbiol, 2017. **2**: p. 16269.
- 333 20. Gold, V.A., et al., *Structure of a type IV pilus machinery in the open and closed state*.
334 Elife, 2015. **4**.
- 335 21. Schlesner, M., et al., *Identification of Archaea-specific chemotaxis proteins which*
336 *interact with the flagellar apparatus*. BMC Microbiol, 2009. **9**: p. 56.
- 337 22. Abrusci, P., et al., *Architecture of the major component of the type III secretion system*
338 *export apparatus*. Nat Struct Mol Biol, 2013. **20**(1): p. 99-104.
- 339 23. Meyer, C., et al., *The Iho670 fibers of Ignicoccus hospitalis are anchored in the cell by a*
340 *spherical structure located beneath the inner membrane*. J Bacteriol, 2014. **196**(21): p.
341 3807-15.
- 342 24. Dobro, M.J., et al., *Electron cryotomography of ESCRT assemblies and dividing*
343 *Sulfolobus cells suggests that spiraling filaments are involved in membrane scission*. Mol
344 Biol Cell, 2013. **24**(15): p. 2319-27.
- 345 25. Wollert, T., et al., *Membrane scission by the ESCRT-III complex*. Nature, 2009.
346 **458**(7235): p. 172-7.
- 347 26. Engelhardt, H., S.C. Schuster, and E. Baeuerlein, *An archimedean spiral: the basal disk*
348 *of the Wolinella flagellar motor*. Science, 1993. **262**(5136): p. 1046-8.
- 349 27. Laloux, G. and C. Jacobs-Wagner, *How do bacteria localize proteins to the cell pole?* J
350 Cell Sci, 2014. **127**(Pt 1): p. 11-9.
- 351 28. Ebersbach, G., et al., *A self-associating protein critical for chromosome attachment,*
352 *division, and polar organization in caulobacter*. Cell, 2008. **134**(6): p. 956-68.
- 353 29. Bowman, G.R., et al., *A polymeric protein anchors the chromosomal origin/ParB*
354 *complex at a bacterial cell pole*. Cell, 2008. **134**(6): p. 945-55.
- 355 30. Bowman, G.R., et al., *Oligomerization and higher-order assembly contribute to sub-*
356 *cellular localization of a bacterial scaffold*. Mol Microbiol, 2013. **90**(4): p. 776-95.
- 357 31. Yamaichi, Y., et al., *A multidomain hub anchors the chromosome segregation and*
358 *chemotactic machinery to the bacterial pole*. Genes Dev, 2012. **26**(20): p. 2348-60.
- 359 32. Butan, C., et al., *Spiral architecture of the nucleoid in Bdellovibrio bacteriovorus*. J
360 Bacteriol, 2011. **193**(6): p. 1341-50.
- 361 33. Raddi, G., et al., *Three-dimensional structures of pathogenic and saprophytic Leptospira*
362 *species revealed by cryo-electron tomography*. J Bacteriol, 2012. **194**(6): p. 1299-306.
- 363 34. Wolf, S.G., et al., *DNA protection by stress-induced biocrystallization*. Nature, 1999.
364 **400**(6739): p. 83-5.
- 365 35. Teramoto, J., et al., *A novel nucleoid protein of Escherichia coli induced under*
366 *anaerobic growth conditions*. Nucleic Acids Res, 2010. **38**(11): p. 3605-18.
- 367 36. Lim, C.J., et al., *The nucleoid-associated protein Dan organizes chromosomal DNA*
368 *through rigid nucleoprotein filament formation in E. coli during anoxia*. Nucleic Acids
369 Res, 2013. **41**(2): p. 746-53.
- 370 37. Spaans, S.K., J. van der Oost, and S.W. Kengen, *The chromosome copy number of the*
371 *hyperthermophilic archaeon Thermococcus kodakarensis KOD1*. Extremophiles, 2015.
372 **19**(4): p. 741-50.

- 373 38. Jeon, S.J., et al., *Unique nucleoid structure during cell division of Thermococcus*
374 *kodakaraensis KOD1*. J Biosci Bioeng, 2001. **91**(1): p. 40-3.
- 375 39. Briegel, A., et al., *Structural conservation of chemotaxis machinery across Archaea and*
376 *Bacteria*. Environ Microbiol Rep, 2015. **7**(3): p. 414-9.
- 377 40. Tivol, W.F., A. Briegel, and G.J. Jensen, *An improved cryogen for plunge freezing*.
378 *Microsc Microanal*, 2008. **14**(5): p. 375-9.
- 379 41. Zheng, S.Q., et al., *UCSF tomography: an integrated software suite for real-time electron*
380 *microscopic tomographic data collection, alignment, and reconstruction*. J Struct Biol,
381 2007. **157**(1): p. 138-47.
- 382 42. Kremer, J.R., D.N. Mastronarde, and J.R. McIntosh, *Computer visualization of three-*
383 *dimensional image data using IMOD*. J Struct Biol, 1996. **116**(1): p. 71-6.
- 384 43. Agulleiro, J.I. and J.J. Fernandez, *Fast tomographic reconstruction on multicore*
385 *computers*. Bioinformatics, 2011. **27**(4): p. 582-3.
- 386 44. Nicastro, D., et al., *The molecular architecture of axonemes revealed by cryoelectron*
387 *tomography*. Science, 2006. **313**(5789): p. 944-8.
- 388

389

390 **FIGURE LEGENDS**

391 **Figure 1. Cytoplasmic conical structures in *Thermococcus kodakaraensis*.** (A) A
392 tomographic slice shows a side view of a conical structure (c) in the cytoplasm, rotated and
393 enlarged in (B). (C) A tomographic slice shows a side view of the cone in another cell,
394 highlighting the subunit texture along the edge of the cone (arrowheads). (D, E) Top views of a
395 cone at different heights show the inner ring (r; enlarged in inset to highlight 19-subunit
396 structure) and outer cone. (F-H) Sequential slices through a side view of a cone in a lysed cell
397 show the relative location of the ring in the cone. (I, J) Different views of a 3D segmentation of
398 the cone shown in (A), embedded in a tomographic slice. s, S-layer; m, membrane; a, archaella;
399 rib, ribosomes; rez, ribosome-excluding zone. Scale bars 100 nm; segmentation not to scale.

400

401 **Figure EV1. Additional examples of conical structures in *T. kodakaraensis* cells.** (A) shows
402 sequential tomographic slices (1-3) at different heights through a side view of the cone.

403 Additional examples of cones in intact **(B-C)** and lysed **(D-E)** cells are shown below. s, S-layer;
404 m, membrane; c, conical structure; a, archaella; r, ring. Scale bars 100 nm.

405

406 **Figure 2. Cones are associated with chemosensory arrays, ribosome-excluding zones and**

407 **filament bundles.** Tomographic slices show side **(A)** and top **(B, C)** views of cones (c) in three

408 cells, highlighting associated chemosensory arrays (ca), ribosome-excluding zones (rez) and

409 filament bundles (f). For a slice-by-slice view through the tomogram shown in **(A)**, see Movie

410 S1. **(D)** and **(E)** show different views of a 3D segmentation of the structures shown in **(C)**, with

411 the conical structure in blue and the filament bundle in red. s, S-layer; m, membrane; a,

412 archaellum; o, other filaments. Scale bar 100 nm; segmentation not to scale.

413

414 **Figure EV2. Double cone structure observed in *T. kodakaraensis*.** A tomographic slice

415 through a side view shows two associated conical structures (c1 and c2), both associated with

416 archaella (a). Scale bar 100 nm.

417

418 **Figure 3. Archaellum orientation with respect to the cell envelope. (A-D)** show tomographic

419 slices through side views of cones. White lines show the angle of the archaellum with respect to

420 the surface layer, and red dashed lines show the conserved distance from the archaellum at the

421 membrane to the cone. Schematic in **(E)** depicts the 44 nm distance from the cone to the basal

422 body in the membrane for archaella at different radial positions along the cone. Since different

423 radial positions on the cone are located at different distances from the membrane (shorter at the

424 tip and longer at the base), this results in a range of archaellar orientations in the cell envelope.

425 Scale bar 100 nm.

426

427 **Figure EV3. Association of cones with the archaellar bundle.** (A) and (B) show tomographic
428 slices through two cells, highlighting the association between the cone and the archaella. (C) and
429 (D) show 3D segmentations of the cells in (A) and (B), respectively, with cones in blue and
430 archaella in red, embedded in tomographic slices. (E) Tomographic slices of individual
431 archaella show the varying orientations of archaella with respect to the cell envelope, as well as
432 apparent connections to the cone. Scale bars 100 nm in (A) and (B), 50 nm in (E); segmentations
433 not to scale.

434

435 **Figure 4. Structure of the *T. kodakaraensis* archaellum.** (A) A sub-tomogram average of the
436 archaellum reveals structural features, including four layers of density in the cytoplasm (L1-L3,
437 cone). CM, cytoplasmic membrane. The speculated identity of densities in the archaellum is
438 proposed: archaellum fiber = FlaA/B flagellins; integral membrane density = FlaJ; L1 = FlaI;
439 L2/L3/cone = FlaH/FlaC/D/E. (B) For comparison, a subtomogram average of the type IVa
440 pilus machine from *Myxococcus xanthus* is shown (adapted with permission from [8]). Arrows
441 indicate components with recognized homology. OM, outer membrane; IM, inner membrane.
442 Scale bar 10 nm.

443

444 **Figure EV4. Individual particles from the subtomogram average show heterogeneity in the**
445 **L3 density and angle of cone density.** The L3 density appears as either two dots of similar
446 (first two panels) or different intensity (third panel), a single dot (fourth panel), or a dot and an
447 extended line (fifth panel). Scale bar 10 nm.

448

449 **Figure 5. Schematic comparing organization of the related archaellum and type IVa pilus**
450 **basal bodies.** In the bacterial T4P (**right**), an integrated system of components spanning the
451 outer and inner membranes (OM, IM) uses the peptidoglycan cell wall (PG) to brace the ATPase,
452 allowing rotation of PilC (orange) in the membrane to assemble the pilus fiber. In the *T.*
453 *kodakaraensis* archaellum (**left**), our results suggest that an integrated system of components
454 extends from the single membrane (CM) inward to a large conical structure in the cytoplasm to
455 similarly brace the ATPase. Sensory components (purple) are proposed to be located in the
456 periplasm for the T4P and the cytoplasm for the archaellum.

Figure 1

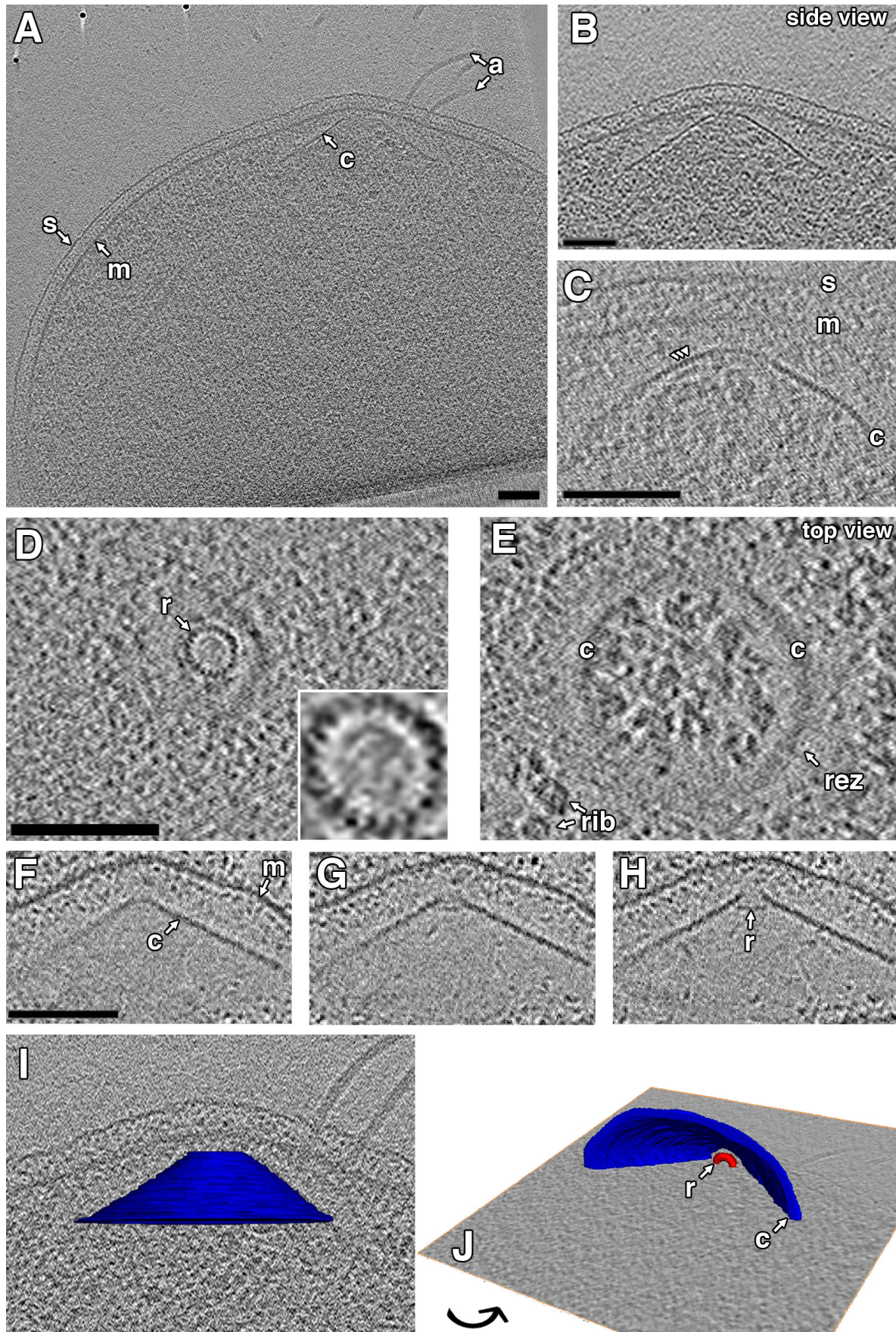


Figure EV1

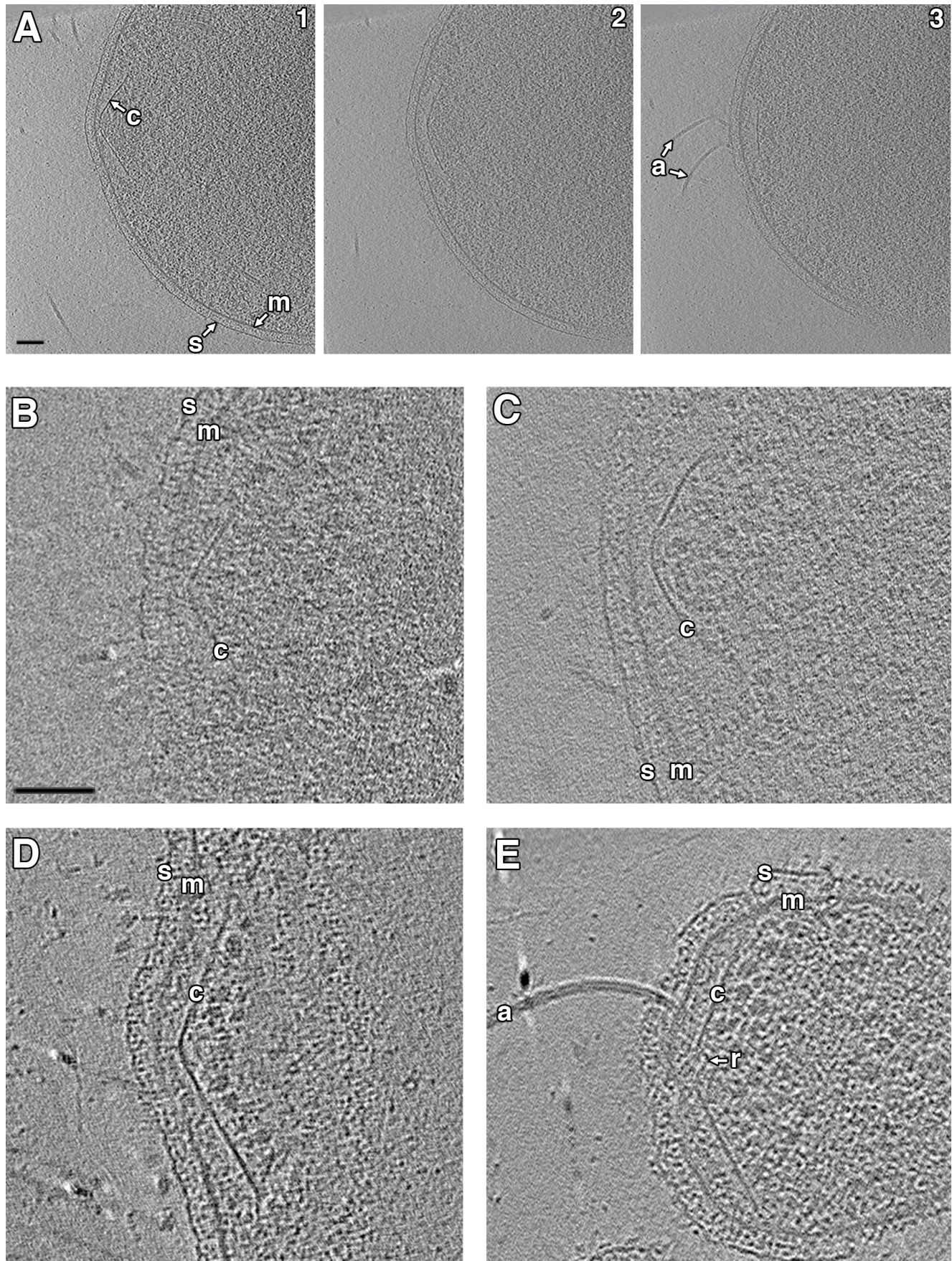


Figure 2

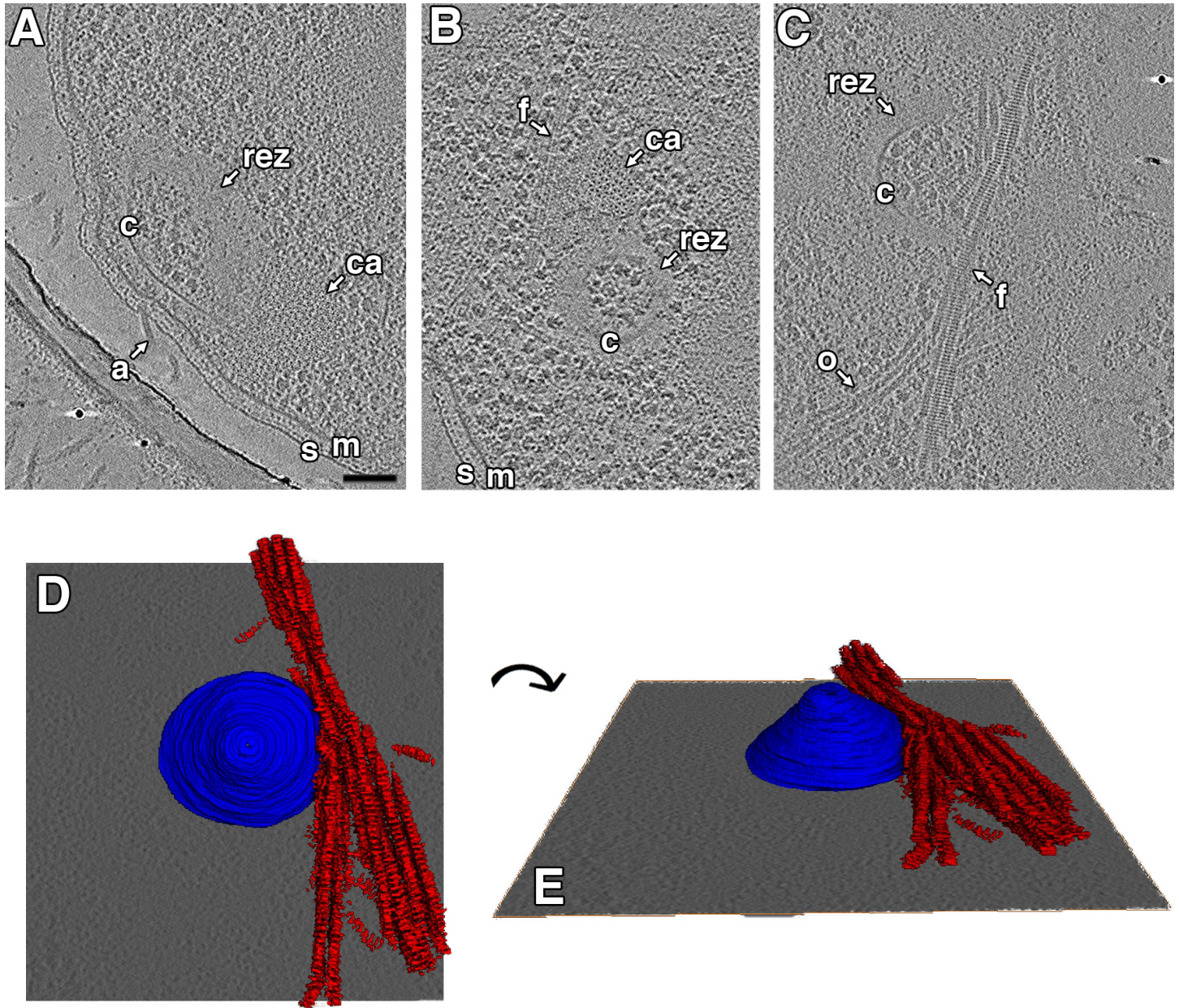


Figure EV2

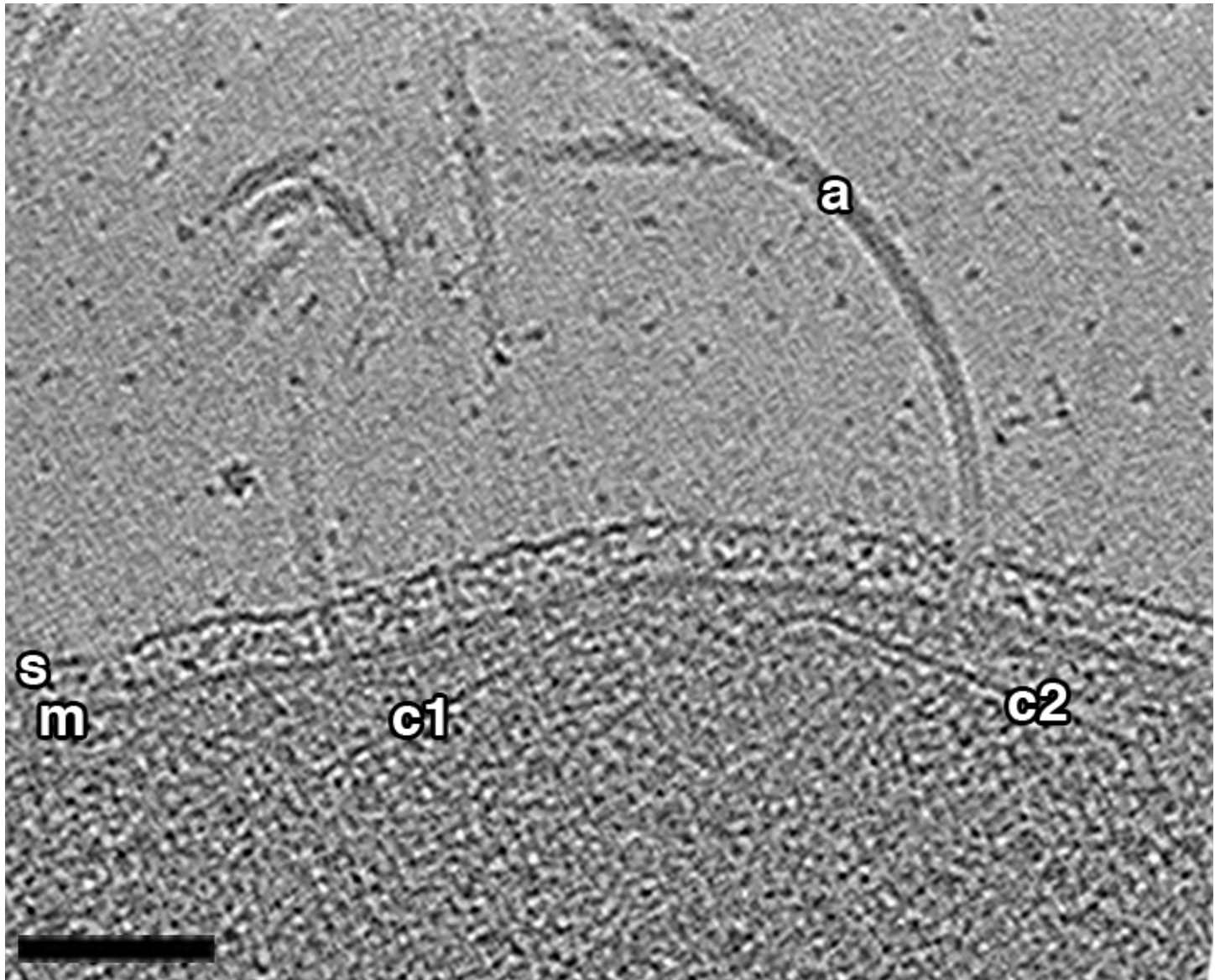


Figure 3

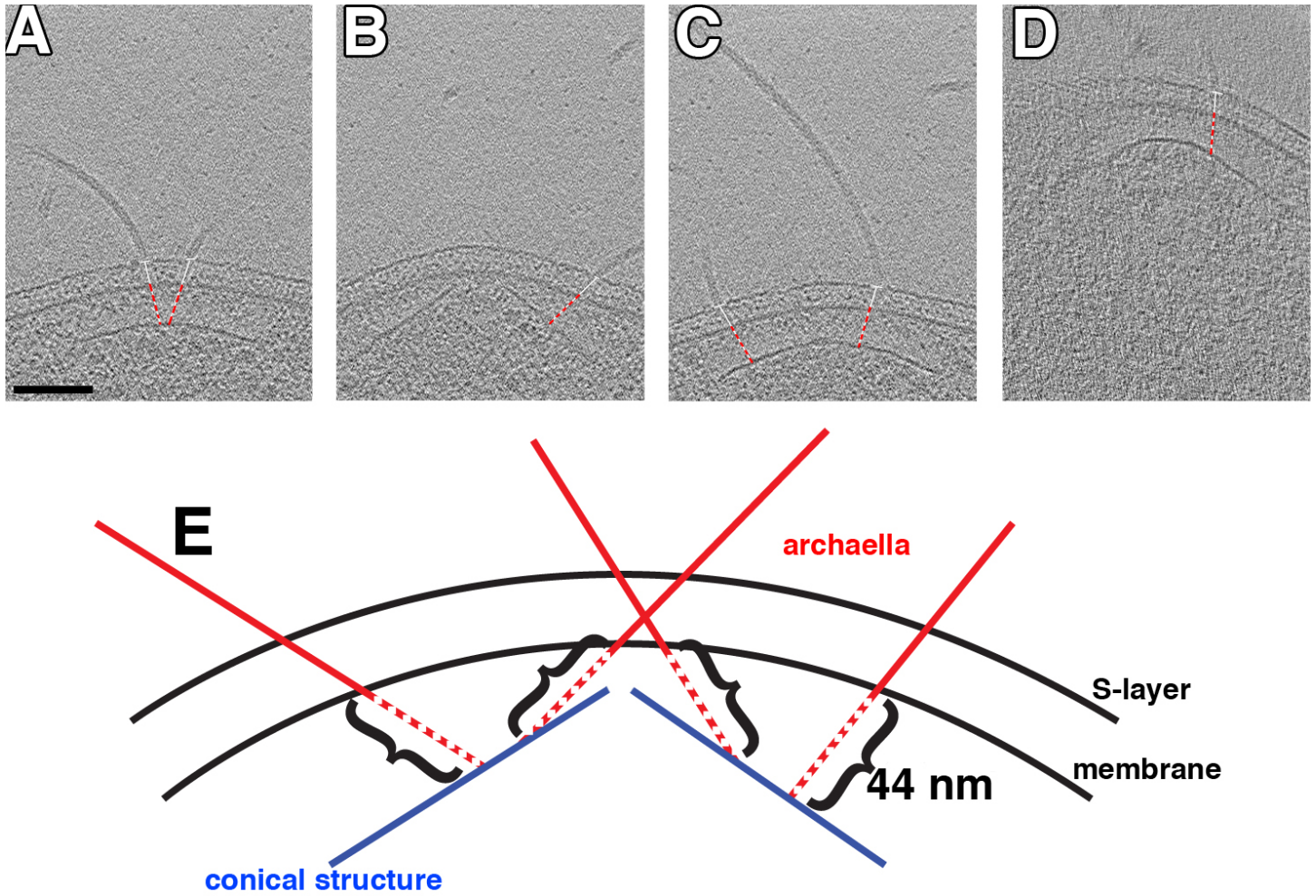


Figure EV3

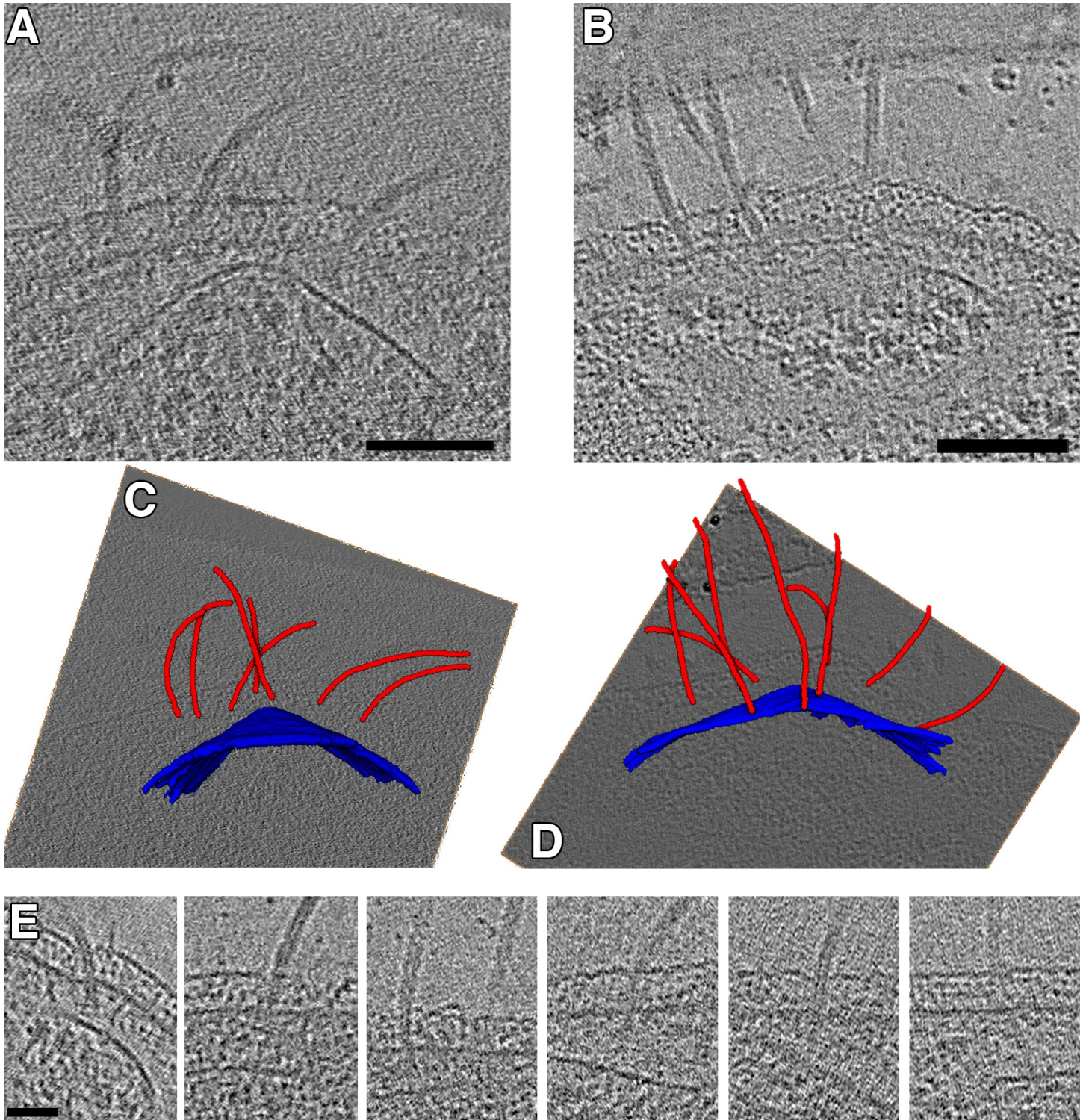


Figure 4

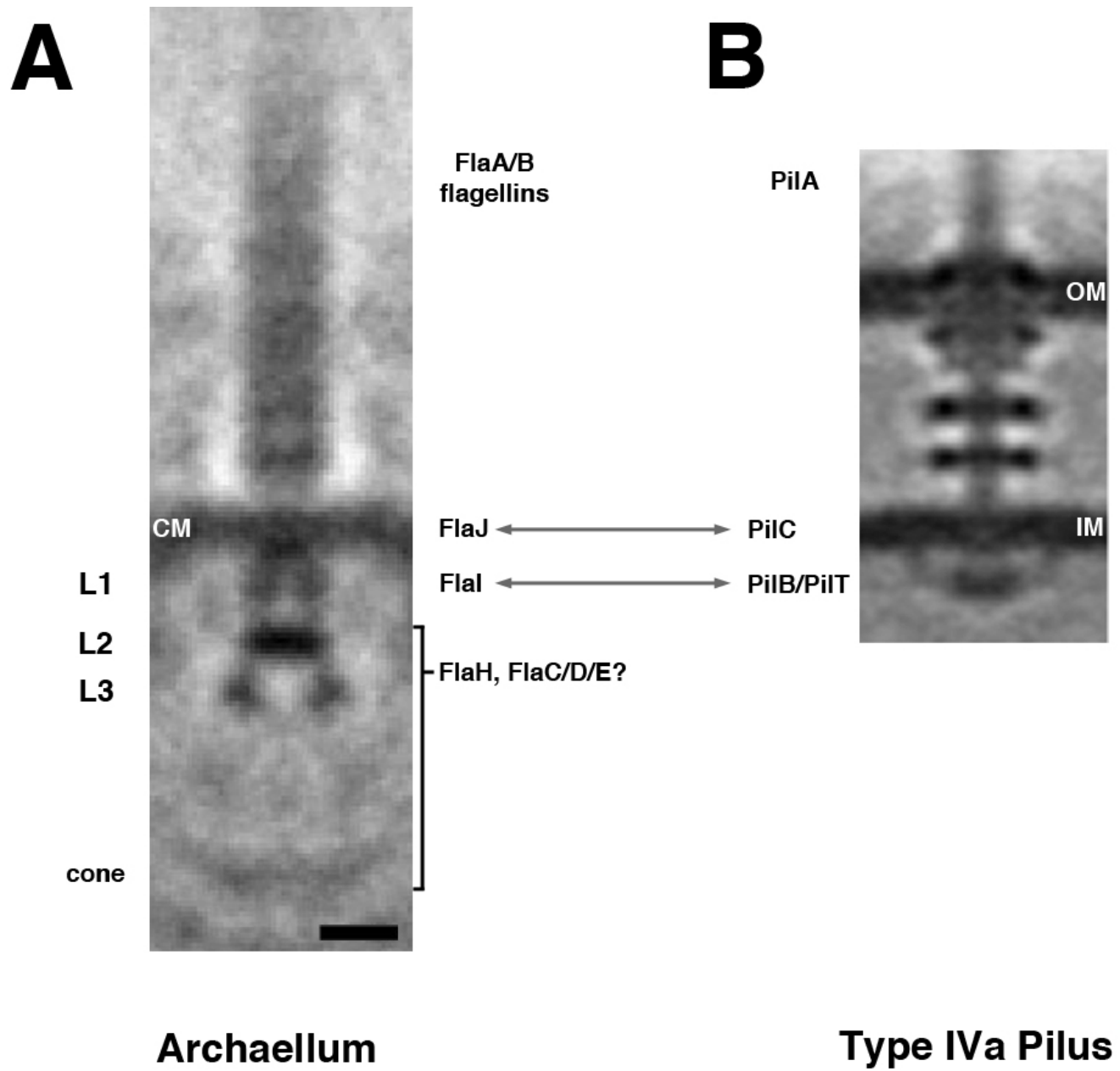


Figure EV4

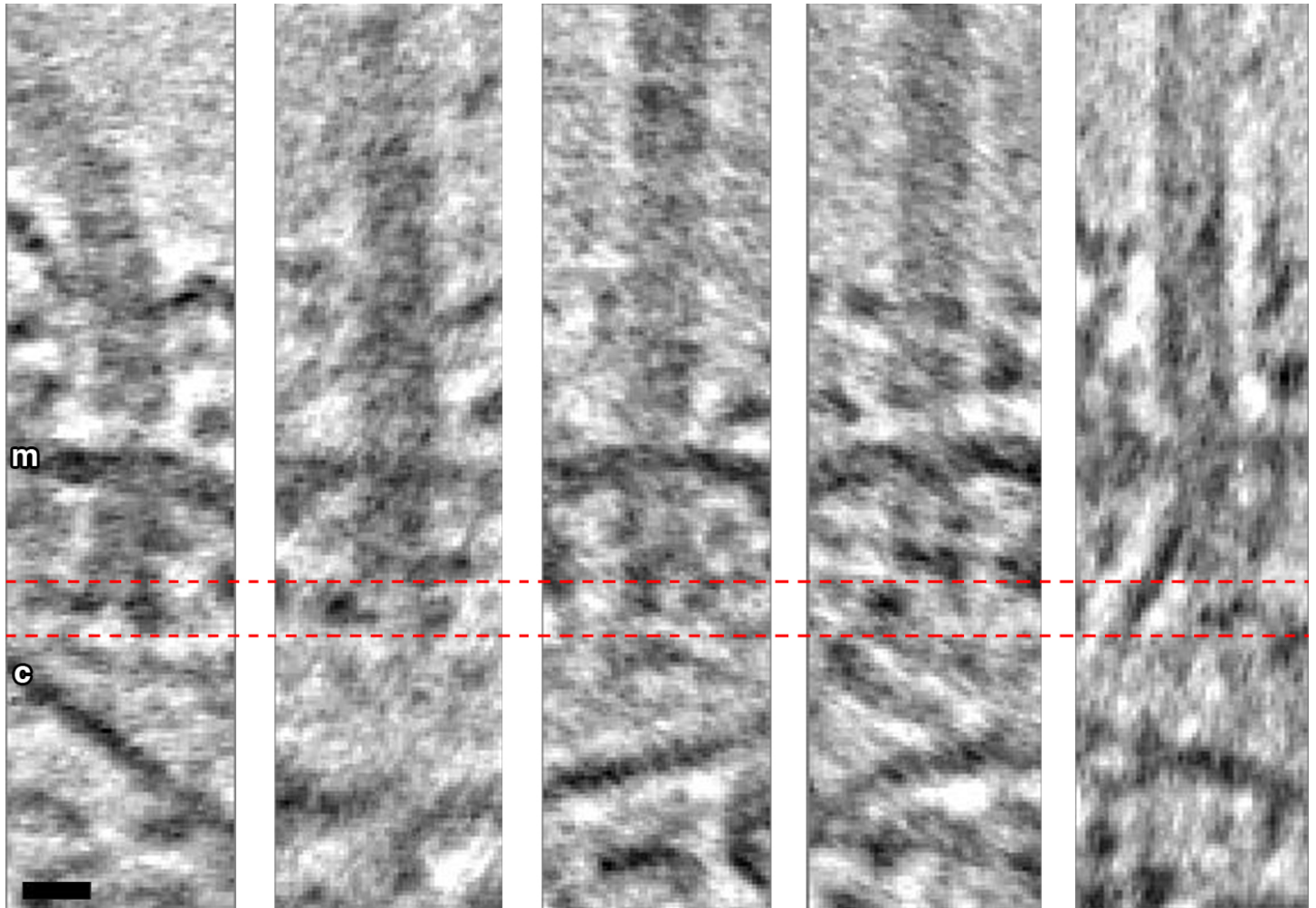


Figure 5

